Inorg. Chem. **2002**, *41*, 4363–4370

Synthesis, Magnetic Properties, and Electronic Spectra of Bis(β-diketonato)chromium(III) and Nickel(II) Complexes with a Chelated Imino Nitroxide Radical: X-ray Structures of $[Cr(acaMe)_2(IM2py)]PF_6$ and $[Ni(acac)_2(IM2py)]$

Yasunori Tsukahara, Takayuki Kamatani, Atsushi Iino, Takayoshi Suzuki, and Sumio Kaizaki*

Department of Chemistry, Graduate School of Science, Osaka University, Toyonaka, Osaka, 560-0043, Japan

Received December 14, 2001

Two new series of each of four Cr(III) and Ni(II) imino nitroxide complexes with various kinds of β-diketonates, [Cr(β-diketonato)$_2$(IM2py)]PF_6, and [Ni(β-diketonato)$_2$(IM2py)] (IM2py = 2-(2′-(pyridyl)-4,4,5,5-tetramethyl-4,5-dihydro-1*H*-imidazol-1-oxy)) have been synthesized, and their structures and magnetic and optical properties have been examined. The X-ray analysis demonstrated that a IM2py ligand coordinated to Cr(III) and Ni(II) acts as a five-membered bidentate chelate. The variable-temperature magnetic susceptibility measurements indicated the antiferromagnetic and ferromagnetic interaction of Cr(III) and Ni(II) with IM2py, respectively, giving a variety of the magnetic coupling constant *J* values with varying the β-diketonato ligands. The UV–vis shoulders around (19–20) $\times 10^3$ and (17–18) $\times 10^3$ cm^{-1} for the Cr(III) and Ni(II) complexes, respectively, characteristic of the IM2py complexes were assigned to the metal–ligand charge-transfer transitions, Cr(t_{2g})-SOMO(π*) and Ni(e_g)-SOMO(π*) MLCT in terms of the resonance Raman spectra and the variable-temperature absorption spectra. The absorption components centered around (13–14) $\times 10^3$ cm^{-1} for the Cr(III) and Ni(II) complexes were due to the formally spin-forbidden d–d transition within the t_{2g} and e_g subshells, associated with the intensity enhancement. The spectroscopic behavior with varying the β-diketonato ligands is discussed in connection with the antiferromagnetic or ferromagnetic coupling constant *J* values on the basis of the exchange mechanism along with the coligand effect.

Introduction

A number of paramagnetic transition metal complexes with nitronyl or imino nitroxide radicals such as several derivatives of 4,4,5,5-tetramethyl-4,5-dihydro-1*H*-imidazolyl-3-oxide-1-oxyl (NIT)[1,2] or 4,4,5,5-tetramethyl-4,5-dihydro-1*H*-imidazol-1-oxy (IM)[3,4] have been investigated from the viewpoint of molecular magnets. On the other hand, electronic spectra of multi-spin systems of paramagnetic transition metal complexes have been extensively investigated;[5−12] e.g., mono-, tri-, tetra-,[9] and one-dimensional ferrimagnetic polynuclear[10] complexes with Cu(II) and Mn(II) ions in connection with magneto-optical molecular devices have been studied where the spin-forbidden transition intensity enhancements on cooling were examined in a quantitative manner. Our recent studies have focused on the magnetic

* Author to whom correspondence should be addressed. E-mail: kaizaki@chem.sci.osaka-u.ac.jp.

(1) (a) Caneschi, A.; Gatteschi, D.; Rey, P. *Prog. Inorg. Chem.* **1991**, *39*, 331 and references therein. (b) Kahn, O. *Molecular Magnetism*; VCH: New York, 1993; (c) Coronado, E.; Dellhaès, P.; Gatteschi, D.; Miller, J. S., Eds. *Molecular Magnetism: From Molecualr Assemblies to the Decives*; NATO ASI Ser. 321; Kluwer Academic Publishers: Dordrecht, The Netherlands, 1996.
(2) Luneau, D.; Risoan, G.; Rey, P.; Grand, A.; Caneschi, A.; Gatteschi, D.; Laugier, J. *Inorg. Chem.* **1993**, *32*, 5616.
(3) Luneau, D.; Rey, P.; Laugier, J.; Belorizky, E.; Cogne, A. *Inorg. Chem.* **1992**, *31*, 3578.
(4) (a) Luneau, D.; Laugier, J.; Rey, P.; Ulrich, G.; Ziessel, R.; Legoll, P.; Drillon, M. *J. Chem. Soc., Chem. Commun.* **1994**, 741. (b) Romero, F. M.; Luneau, D.; Ziessel, R. *J. Chem. Soc., Chem. Commun.* **1998**, 551. (c) Luneau, D.; Romero, F. M.; Ziessel, R. *Inorg. Chem.* **1998**, *37*, 5078.
(5) Marvilliers, A.; Pei, Y.; Boquera, J. C.; Vostrikova, K. E.; Paulsen, C.; Rivière, E.; Audière, J.-P.; Mallah, T. *Chem. Commun.* **1999**, 1951.
(6) Vostrikova, K. E.; Luneau, D.; Wernsdorfer, W.; Rey, P.; Verdaguer, M. *J. Am. Chem. Soc.* **2000**, *122*, 718.
(7) Güdel, H. U. In *Magnetic-Structural Correlations in Exchange Coupled Systems*; Willet, R. D., Gatteschi, D., Kahn, O., Eds.; Reidel: Dordrecht, The Netherlands, 1985;, p 297.
(8) McCarthy, P. U.; Güdel, H. U. *Coord. Chem. Rev.* **1988**, *88*, 69.
(9) (a) Bellitto, C.; Day, P. *J. Chem. Soc., Dalton Trans.* **1978**, 1207. (b) Bellitto, C.; Day, P. *J. Chem. Soc., Dalton Trans.* **1986**, 847. (c) Bellitto, C.; Day, P. *J. Mater. Chem.* **1992**, *2*, 265.

10.1021/ic011282m CCC: $22.00
Published on Web 07/24/2002

Chart 1

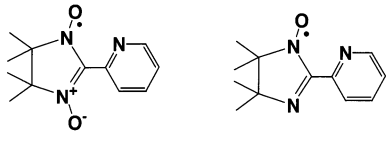

(a) NIT2py (b) IM2py

and spectroscopic properties of [M(β-diketonato)$_2$(NIT2py)]$^{n+}$ (M = Ni(II)[13−15] and Cr(III)[13,16]), as well as of [M^{II}Cl$_2$(IM2py)$_2$] complexes (M = Zn, Ni, Mn, Co)[17] and tetrahedral complexes [M^{II}Cl$_2$(NITmepy or IMmepy)] (M = Zn, Co, Ni),[18] following the related diamagnetic Co(III) complexes[19] with unidentate NITnpy and IMnpy (n = 3 and 4) and the chelated IM2py lanthanide(III) complexes.[20] For the NIT2py Ni(II) and Cr(III) β-diketonates complexes, the relations have been examined between the antiferromagnetic exchange coupling constants and the spin-forbidden d−d transition intensities[14,16] or the NMR contact shifts,[15] demonstrating the coligand effect. There remain open questions on the coligand effect and quantitative complementarity between optical and magnetic properties. To get some clues for these problems, comparison of the magnetic and optical properties between the NIT2py complexes and the IM2py complexes is inevitable. However, there is no magnetic and optical study on the IM2py Ni(II) and Cr(III) β-diketonate complexes so far.

In this article, the synthesis of a series of Cr(III) and Ni(II) IM2py complexes with various β-diketonates and their magnetic and spectroscopic properties together with the X-ray structural analysis are described in comparison with those of the Cr(III) and Ni(II) NIT2py complexes.[14,16]

Experimental Section

Ligands. The radical ligand IM2py was prepared by the literature method.[21] The β-diketones were commercially available (β-diketone = Hacac (2,4-pentanedione), Hdbm (1,3-diphenyl-1,3-propanedione), Hbzac (1-phenyl-1,3-butanedione), HacaMe (3-methyl-2,4-pentanedione), HacaPh (3-phenyl-2,4-pentanedione), Hhfac (1,1,1,-5,5,5-hexafluoro-2,4-pentanedione), and Htfac (1,1,1-trifluoro-2,4-pentanedione).

Materials: Starting and Reference Complexes. The starting complexes [Cr(β-diketonato)$_2$(H$_2$O)$_2$]BF$_4$ [16] and [Ni(β-diketonato)$_2$(H$_2$O)$_2$][22] and the reference complexes [Cr(acac)$_2$(en)]PF$_6$[23] and [Ni(acac)$_2$(tmen)][24] were synthesized according to literature methods.

Syntheses of IM2py Complexes: (1) [Cr(acaMe)$_2$(IM2py)]PF$_6$ (3a). To a solution of 1 mmol of [Cr(acaMe)$_2$(H$_2$O)$_2$]BF$_4$ in 50 mL of CH$_3$CN was added 1 mmol of IM2py with stirring in an ice−methanol bath at −15 °C. After 3 h of stirring, the solution was evaporated under reduced pressure. The residue was dissolved in 50 mL of EtOH, and to this solution was added 1 mmol of NaPF$_6$. After 6 h of stirring, the solution was evaporated under reduced pressure around 15 °C. The crude product was obtained by adding dichloromethane. The residue was dissolved in 10 mL of CHCl$_3$. This solution was loaded on a preparative HPLC (LC-908 (Japan Analytical Industry Co. Ltd.)), and the column was eluted with CHCl$_3$. The first band was found to be the desired product of [Cr(acaMe)$_2$(IM2py)]$^+$. After the eluate was condensed, orange red needlelike crystals were obtained by a vapor diffusion method in dichloromethane−ether.

The other β-diketonato complexes [Cr(β-diketonato)$_2$(IM2py)]PF$_6$ (β-diketonato = acac (**1a**), dbm(**2a**), and acaPh (**4a**)) were obtained by a method similar to that for the acaMe complex.

(2) [Ni(acac)$_2$(IM2py)] (1b). To a suspension of 1 mmol of [Ni(acac)$_2$(H$_2$O)$_2$] in 20 mL of Et$_2$O was added 1 mmol of IM2py with stirring at room temperature. [Ni(acac)$_2$(H$_2$O)$_2$] was not dissolved in Et$_2$O, but IM2py was dissolved in Et$_2$O. This suspension was stirred for 1 h. Then, the solid was dissolved and the solution became clear. To the solution was added 30 mL of *n*-heptane. This was evaporated under reduced pressure. When the crude crystals began to deposit, evaporation was stopped. After the crude crystals were dissolved again by warming, the solution was allowed to stand in a refrigerator. The solid was collected on a glass filter. Complex [Ni(acac)$_2$(IM2py)] was obtained as deep brown platelike crystals by a vapor diffusion method in dichloromethane−ether. The other β-diketonato complexes [Ni(β-diketonato)$_2$(IM2py)] (β-diketonato = bzac (**2b**), hfac (**3b**), and tfac(**4b**)) were prepared by a method similar to that for the acac complex.

Crystallography. An orange-red crystal of [Cr(acaMe)$_2$(IM2py)]PF$_6$ with approximate dimensions of 0.35 × 0.22 × 0.06 mm^3 was glued on the top of a glass fiber with epoxy resin. The X-ray intensities ($2\theta_{max}$ = 55) were collected on a Rigaku RAXIS-RAPID Imaging Plate.

A deep brown crystal of [Ni(acac)$_2$(IM2py)] was sealed in a glass capillary with epoxy resin. The X-ray intensities ($2\theta_{max}$ = 55) were collected on an automated Rigaku AFC-5R four-circle diffractometer.

Absorption corrections were applied by a multiscan method.[25] The structure was solved by the direct method with the SHELXS86 program[26] and refined on F^2 with all independent reflections with the SHELXL97 program.[26] All calculations were carried out with a TeXsan[27] software package.

(10) (a) Mathonieres, C.; Kahn, O.; Daran, J. C.; Hilbig, H.; Kohler, F. H. *Inorg. Chem.* **1993**, *32*, 4057. (b) Mathonieres, C.; Kahn, O. *Inorg. Chem.* **1994**, *33*, 2103. (c) Cador, C.; Mathonieres, C.; Kahn, O. *Inorg. Chem.*, **1997**, *36*, 1923. (d) Cador, C.; Mathonieres, C.; Kahn, O.; Costes, J. P.; Verelst, M.; Lecante, P. *Inorg. Chem.* **1999**, *38*, 2643. (e) Cador, C.; Mathonieres, C.; Kahn, O. *Inorg. Chem.* **2000**, *39*, 3799.

(11) Benelli, C.; Dei, A.; Gatteschi, D.; Güdel, H. U.; Pardi, L. *Inorg. Chem.* **1989**, *28*, 3089.

(12) Sokolowski, A.; Bothe, E.; Bill, E.; Weyhermuller, T.; Wieghardt, K. *J. Chem. Soc., Chem. Commun.* **1996**, 1671.

(13) Yoshida, T.; Kanamori, K.; Takamizawa, S.; Mori, W.; Kaizaki, S. *Chem. Lett.* **1997**, 603.

(14) Yoshida, T.; Suzuki, T.; Kanamori, K.; Kaizaki, S. *Inorg. Chem.* **1999**, *38*, 1059.

(15) Yoshida, T.; Kaizaki, S. *Inorg. Chem.* **1999**, *38*, 1054.

(16) Tsukahara, Y.; Iino, A.; Yoshida, T.; Suzuki, T.; Kaizaki, S. *J. Chem. Soc., Dalton Trans.* **2002**, 181.

(17) Yamamoto, Y.; Suzuki T.; Kaizaki, S. *J. Chem. Soc., Dalton Trans.* **2001**, 1566.

(18) Yamamoto, Y.; Suzuki T.; Kaizaki, S. *J. Chem. Soc., Dalton Trans.* **2001**, 2943.

(19) (a) Suzuki, T.; Ogita, M.; Kaizaki, S. *Acta Crystallogr., Sect. C* **2000**, *56*, 532. (b) Ogita, M.; Yamamoto, Y.; Suzuki, T.; Kaizaki, S. *Eup. J. Inrog. Chem.* **2002**, 886.

(20) (a) Tsukuda, T.; Suzuki, T.; Kaizaki, S., *J. Chem. Soc., Dalton Trans.* **2002**, 1721. (b) Tsukuda, T.; Suzuki, T.; Kaizaki, S. *Mol. Cryst. Liq. Cryst.*, in press.

(21) Ullman, E. F.; Call, L.; Osiecki, J. H. *J. Org. Chem.* **1970**, *35*, 3623.

(22) Charles, R. G.; Pawlikowsky, M. A. *J. Phys. Chem.* **1958**, *62*, 440.

(23) Kaizaki, S.; Hidaka, J.; Shimura, Y. *Inorg. Chem.* **1973**, *12*, 135.

(24) (a) Fukuda, Y.; Sone, K. *Bull. Chem. Soc. Jpn.* **1970**, *43*, 2282. (b) Fukuda, Y.; Sone, K. *J. Inorg. Nucl. Chem.* **1972**, *34*, 2315. (c) Fukuda, Y.; Sone, K. *J. Inorg. Nucl. Chem.* **1975**, *37*, 455.

(25) Higashi, T. *Abscor-Empirical Absorption Correction based on Fourier Series Approximation*;.Rigaku Corporation: Tokyo, Japan. 1995.

(26) Sheldrick, G. M. *SHELXS-86*, Program for Crystal Structure Determination; University of Göttingen: Göttingen, Germany, 1986.

(27) *TEXSAN*, Single-Crystal Structure Analysis Software, Ver. 1.7; Molecular Structure Corperation: The Woodland, TX, 1995.

Table 1.

	compds	found (calcd) /% C	H	N
1a	$[Cr(acac)_2(IM2py)]PF_6$	43.7 (43.1)	5.14 (4.93)	6.67 (6.85)
2a	$[Cr(dbm)_2(IM2py)]PF_6$	58.0 (58.5)	4.44 (4.44)	4.86 (4.88)
3a	$[Cr(acaMe)_2(IM2py)]PF_6$	45.1(44.9)	5.34 (5.34)	6.75 (6.55)
4a	$[Cr(acaPh)_2(IM2py)]PF_6$	51.6 (53.3)	4.82(5.00)	5.20 (5.49)
1b	$[Ni(acac)_2(IM2py)]$	55.4 (55.6)	6.26 (6.36)	8.91 (8.84)
2b	$[Ni(bzac)_2(IM2py)]$	64.1 (64.1)	5.88(5.72)	6.89 (7.01)
3b	$[Ni(hfac)_2(IM2py)]$	38.0 (38.2)	2.68(2.63)	5.88 (6.08)
4b	$[Ni(tfac)_2(IM2py)]$	45.3(45.3)	4.12(4.15)	7.32 (7.21)

Table 2. Crystallographic Data

	$[Cr(acaMe)_2(IM2-py)]PF_6$	$[Ni(acac)_2(IM2-py)]$
formula	$C_{24}H_{34}F_6N_3CrPO_5$	$C_{22}H_{30}N_3NiO_5$
fw	641.515	475.20
T, °C	−50	23
cryst syst	monoclinic	monoclinic
space group	$P2_1/c$	$C2/c$
a, Å	10.7128(4)	29.018(3)
b, Å	15.7194(5)	10.095(3)
c, Å	17.1131(6)	17.972(4)
β, deg	94.473(2)	111.45(1)
V, Å^3	2873.05(17)	4900(2)
Z	4	8
λ, Å	0.71069	0.71072
ρ_{calcd}, g cm^{-3}	1.483	1.288
μ(Mo Kα), cm^{-1}	0.531	0.827
$R1$[a]	0.074	0.045
$wR2$[b]	0.2382	0.135

[a] $R1 = \sum||F_o| - |F_c||/\sum|F_o|$. [b] $wR2 = [\sum w(F_o^2 - F_c^2)^2/\sum wF_o^2]^{1/2}$.

Measurements. UV−vis absorption spectra were obtained on a Perkin-Elmer Lambda 19 spectrophotometer. Low-temperature UV−vis absorption spectra were measured at 200, 100, 50, and 10 K by the same spectrophotometer in a film made from cellulose acetate in acetonitrile with an Oxford CF1204 cryostat.

Magnetic susceptibility data were obtained at 2000 Oe between 2 and 300 K by using a SQUID susceptometer (MPMS-5S, Quantum Design). Pascal's constants were used to determine the constituent atom diamagnetism. The inter- and intramolecular magnetic interaction of the hfac complex **3b** were estimated from the remeasured magnetic susceptibility data in terms of the present analysis. The J and J' values were not so much different from those of literature values.[3]

Resonance Raman spectra were measured in the solid state by a Jasco NR1800 Raman spectrophotometer at room temperature, using Ar laser lines (488.00, 514.50 nm), He−Ne laser line (632.80 nm), and dye laser lines (584.47, 606.27 nm) as excitation sources.

Results and Discussion

Preparations and Characterization. The reaction time for the IM2py Cr(III) complexes is shorter than that for the corresponding NIT2py complexes. Thus, the IM2py radical is more easily coordinated to the starting Cr(III) complex than the NIT2py radical. No crystallization solvent as inferred from the elemental analyses in Table 1 suggests the chelation of IM2py ligand on Cr(III) and Ni(II) ions as confirmed by the X-ray analysis (vide infra).

Molecular Structure. The crystallographic data for **3a** ($[Cr(acaMe)_2(IM2py)]PF_6$) and **1b** ($[Ni(acac)_2(IM2py)]$) are listed in Table 2. Selected bond lengths, bond angles, torsion angles, and dihedral angles are summarized in Table 3. As shown in Figures 1 and 2, they are octahedral complexes

Table 3. Selected Bond Distances (Å), Bond Angles (deg), Torsion Angles (deg), and Dihedral Angles (deg) of $[Cr(acaMe)_2(IM2py)]PF_6$ and $[Ni(acac)_2(IM2py)]$.

M	Cr	Ni
	bond distances (Å)	
M−O(21)	1.931(3)	2.026(2)
M−O(22)	1.941(3)	2.016(2)
M−O(41)	1.927(3)	2.020(2)
M−O(42)	1.947(3)	2.020(2)
M−N(1)	2.040(3)	2.151(3)
M−N(3)	2.121(4)	2.103(3)
O(1)−N(2)	1.265(5)	1.266(4)
N(1)−C(1)	1.308(5)	1.280(4)
N(2)−C(3)	1.493(6)	1.492(5)
N(3)−C(8)	1.369(5)	1.351(4)
N(3)−C(12)	1.335(6)	1.329(4)
C(1)−C(8)	1.447(6)	1.466(4)
	bond angles (deg)	
N(1)−M−O(21)	170.85(14)	96.11(10)
N(1)−M−O(22)	91.60(13)	95.06(10)
N(1)−M−O(41)	96.93(14)	169.24(10)
N(1)−M−O(42)	89.96(13)	84.73(10)
N(1)−M−N(3)	78.70(14)	77.51(10)
O(21)−M−O(22)	89.31(12)	90.41(10)
O(21)−M−O(41)	92.16(13)	88.78(9)
O(21)−M −O(42)	89.10(13)	178.84(10)
O(21)−M−N(3)	92.21(13)	88.80(9)
O(22)−M−O(41)	90.43(13)	94.48(10)
O(22)−M−O(42)	178.40(13)	90.31(10)
O(22)−M−N(3)	89.16(13)	172.40(10)
O(41)−M−O(42)	89.74(13)	90.26(10)
O(41)−M−N(3)	175.60(13)	93.06(10)
O(42)−M−N(3)	90.80(13)	90.61(10)
O(1)−N(2)−C(1)	125.8(4)	127.0(3)
C(1)−N(1)−Cr	113.3(3)	111.4(2)
C(2)−N(1)−Cr	136.9(3)	135.6(2)
M−N(3)−C(8)	114.8(3)	118.0(3)
M−N(3)−C(12)	127.3(3)	126.1(2)
	torsion angles (deg)	
N(1)−C(1)−C(8)−N(3)	2.0(6)	−8.0(4)
	dihedral angles (deg)	
plane 1[a] vs plane 2[b]	3.036	9.633
plane 1 vs plane 3[c]	3.199	13.27
plane 2 vs plane 3	2.440	15.57

[a] Plane 1 (N(1), C(1), N(2), O(1)). [b] Plane 2 (N(3), C(8), C(9), C(10), C(11), C(12)). [c] Plane 3 (M, N(1), N(3)).

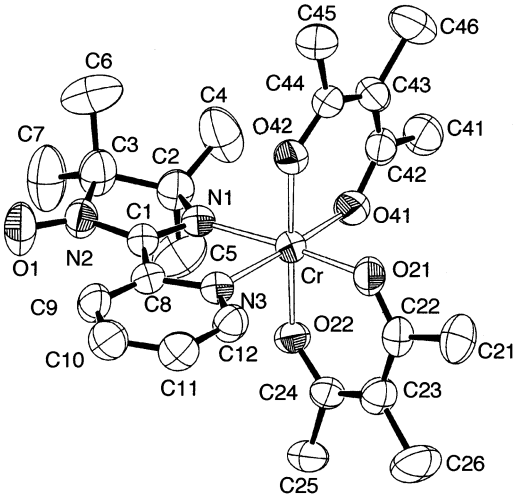

Figure 1. View of the molecular structure of $[Cr(acaMe)_2(IM2py)]PF_6$ (**3a**).

which are coordinated by a five-membered chelate through the pyridyl nitrogen and IM nitrogen of the IM2py together

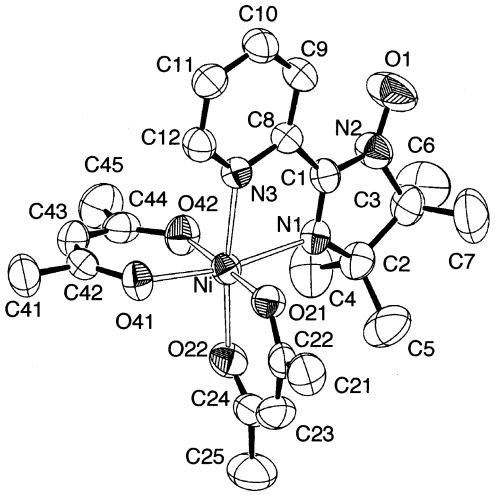

Figure 2. View of the molecular structure of [Ni(acac)$_2$(IM2py)] (**1b**).

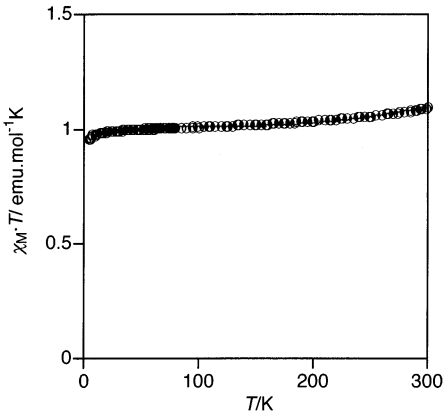

Figure 3. Temperature dependence of the magnetic susceptibilities for [Cr(acac)$_2$(IM2py)]PF_6 (**1a**) (○) in the form of $\chi_M T$ vs T. The solid line represents the best-fit calculated data.

with each of two chelated β-diketonato ligands. The O(1)−N(2) lengths (1.265(5) Å for **3a** and 1.266(4) Å for **1b**) of the IM moiety substantiate the existence of the imino nitroxide radical. As shown in Table 3, the dihedral angles around the coordinated IM2py moiety together with the torsion angle of N(1)−C(1)-C(8)−N(3) for **3a** are much smaller than the corresponding values for [Cr(dpm)$_2$(NIT2py)]-PF_6.[16] This indicates that the IM2py chelate in **3a** is more planar than those in the Cr(III) NIT2py complexes. A similar situation is encountered between the Ni(II) IM2py(**1b**) and NIT2py complexes.[14] As compared with the dihedral and torsion angles around the IM2py moiety in the Cr(III) complex **3a** and the Ni(II) complex **1b**, the IM2py chelate in the Cr(III) complex is more planar than that of the Ni(II) complex as found in the case of the corresponding pair of NIT2py complexes.[14,16] The molecular structures of the other β-diketonato Cr(III) and Ni(II) complexes are expected to be the same as those of **3a** and **1b**, respectively, in view of the similarity in the UV−vis spectral pattern and SQUID magnetic susceptibility as described below.

Magnetic Properties. The products of the molar magnetic susceptibilities (χ_M) and temperature (T) ($\chi_M \cdot T$) vs T plots for [Cr(acac)$_2$(IM2py)]PF_6 are shown in Figure 3. The $\chi_M \cdot T$ products at room temperature are smaller than the calculated values for uncorrelated systems containing a chromium(III) cation and IM2py radical ($S = {}^3/_2 + {}^1/_2$) ($\chi_M \cdot T = 2.25$ emu K mol^{-1}) and decrease on lowering the temperature, suggesting the antiferromagnetic interaction between the Cr(III) and IM2py radical. The other β-diketonato complexes give a similar pattern for the $\chi_M \cdot T$ vs T plots. The magnetic coupling constants J_{obs} involving a Cr(III) ion and IM2py were obtained by least-squares fits for the magnetic susceptibilities χ_M to a two-spin system ($H = -2JS_1 \cdot S_2$; $S_1 = {}^3/_2$, $S_2 = {}^1/_2$)[28] including a Weiss constant θ. The coupling constants J_{obs} with $g =$ ca. 2.0 and $R = 10^{-4}-10^{-5}$ range from −96.4 to −188 cm^{-1} together with $\theta = -0.33$ to −0.06 cm^{-1} as summarized in Table 4 and Table S1. These results show that the intramolecular magnetic interaction in the Cr(III) IM2py complexes is antiferromagnetic as predicted for the corresponding NIT2py complexes[16] and that the intermolecular interaction is small in accordance with that inferred from the long intermolecular distance (∼6 Å) in the crystal packings of complex **3a**.

As shown in Figure 4, the $\chi_M \cdot T$ products for [Ni(acac)$_2$-(IM2py)] at room temperature are larger than the calculated value ($\chi_M \cdot T = 1.375$ emu K mol^{-1}) for uncorrelated systems containing a nickel(II) cation and IM2py and increase on lowering the temperature, suggesting the ferromagnetic interaction between the Ni(II) and IM2py radical. The decrease of the $\chi_M \cdot T$ values at low temperature may result in the intermolecular interaction. The other [Ni(β-diketonato)$_2$-(IM2py)] complexes give similar patterns for the $\chi_M \cdot T$ vs T plots. The J_{obs} for the magnetic interaction between a nickel-(II) ion and IM2py and the intermolecular interaction θ values were estimated by fitting the magnetic susceptibilities χ_M to a two-spin system ($H = -2JS_1 \cdot S_2$; $S_1 = 1$, $S_2 = {}^1/_2$), with $g = 2.13-2.22$ ranging from $J_{obs} = +0.400$ to +95.3 cm^{-1} and from $\theta = -0.25$ cm^{-1} with $R = 10^{-5}$ for **1b** to $\theta = -9$ cm^{-1} with $R = 70 \times 10^{-4}$ for **4b**.

The intermolecular interaction (θ) in the acac complex **1b** is weak as suggested from the long intermolecular distance (6.22 Å). For the tfac complex **4b** with the short intermolecular N−O···O−N distance (3.46 Å) demonstrated by preliminary X-ray analysis, the re-estimated magnetic interaction including the J' value instead of θ is −6.08 cm^{-1} with $R = 9.4 \times 10^{-4}$, in accordance with the case (3.97 Å)[3] for the hfac complex with $J' = -2.80$ cm^{-1}.

The intramolecular magnetic interactions (J) thus obtained between the IM2py complexes of Cr(III) and Ni(II) will be discussed below.

Visible Absorption Spectra: Intraligand and Charge-Transfer Transitions. The spectral characteristics of the IM2py Cr(III) and Ni(II) complexes are different from those of both the IM2py itself and the nonradical Cr(III) and Ni(II) complexes as shown in Figures 5 and 6. The vibronic structure around 20.0×10^3 cm^{-1} for both the Cr(III) and Ni(II) complexes may originate from the intraligand transition, in view of the similarity in intensity and shift behavior for variation of the β-diketonates as well as for the IM2py Co(II), Ni(II), and Ln(III) complexes[17,20] and IM3py and IM4py Co(III) complexes.[19b] New absorption shoulders are

(28) Wojciechowski, W. *Inorg. Chim. Acta* **1967**, *1*, 324.

Table 4. Magnetic and Optical Data of the IM2py Cr(III) and Ni(II) Complexes

	compd	J_{obsd} (g)[a]	ϵ_{SF}[b]	ϵ_{CT}[c]	E_{CT}[d]	ΔE_{CT}[e]	$(\epsilon_{SF}/\epsilon_{CT})(\Delta E_{CT})^2/(E_{CT})$[f]
1a	$[Cr(acac)_2(IM2py)]\ PF_6$	−188 (2.01)	145.9	923.1	19.12	4.96	0.203
2a	$[Cr(dbm)_2(IM2py)]\ PF_6$	−96.4 (2.05)	159.7	1044	19.16	5.13	0.210
3a	$[Cr(acaMe)_2(IM2py)]\ PF_6$	−102 (2.03)	191.1	1367	19.57	5.80	0.241
4a	$[Cr(acaPh)_2(IM2py)]\ PF_6$	−119 (2.01)	184.0	1160	19.57	5.60	0.255
1b	$[Ni(acac)_2(IM2py)]$	41.2 (2.12)	11.6	107.0	17.04	4.32	0.119
2b	$[Nir(bzac)_2(IM2py)]$	0.397 (2.13)	8.91	79.9	17.06	4.34	0.123
3b	$[Ni(hfac)_2(IM2py)]$	95.3 (2.15)	4.86	44.9	17.47	4.64	0.133
4b	$[Ni(tfac)_2(IM2py)]$	71.2 (2.13)	4.92	43.9	17.30	4.46	0.129

[a] Obserbed J values in cm^{-1}. [b] Molar absorption coefficient for the spin-forbidden in $mol^{-1}dm^3cm^{-1}$. [c] Molar absorption coefficient for the MLCT transition in $mol^{-1}dm^3cm^{-1}$. [d] MLCT transition energy in $10^3\ cm^{-1}$. [e] The energy difference between the spin-forbidden and MLCT transition/10^3cm^{-1}. [f] $\propto J_{AF}$ in $10^3\ cm^{-1}$.

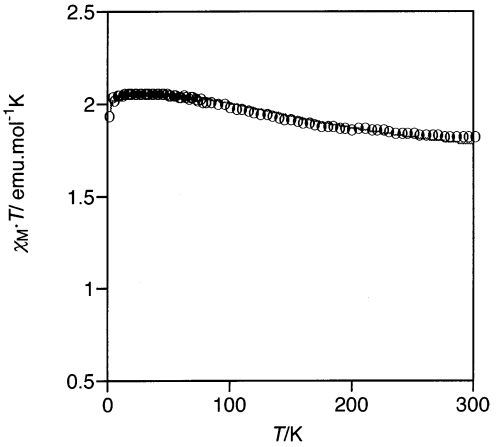

Figure 4. Temperature dependence of the magnetic susceptibilities for $[Ni(acac)_2(IM2py)]$ (**1b**) (○) in the form of $\chi_M T$ vs T. The solid line represents the best-fit calculated data.

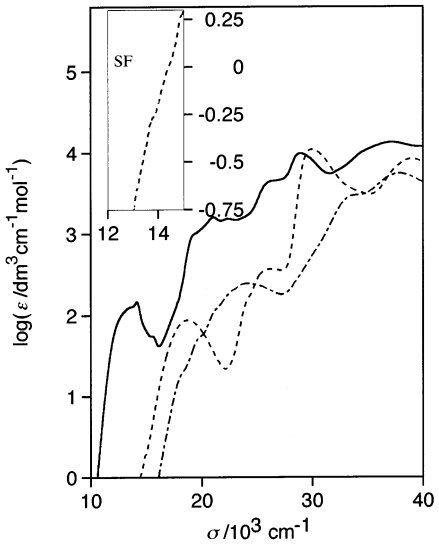

Figure 5. Absorption spectra of $[Cr(acac)_2(IM2py)]PF_6$ (**1a**) (−), $[Cr(acac)_2(en)]PF_6$ (− −), and IM2py (− - −) in CH_3CN at room temperature. Inset: Enlarged absorption curve with the logarithmic ordinate of $[Cr(acac)_2(en)]PF_6$ (− −) in CH_3CN at room temperature.

observed around (19.0−21.0) × 10^3 cm^{-1} for the Cr(III) complexes and (17.0−18.0) × 10^3 cm^{-1} for the Ni(II) complexes. These shoulders may be assigned to neither the intraligand nor the d−d transitions, but to the charge-transfer transitions as supported by the resonance Raman spectra given below.

In the Raman resonance spectra in the region (19.0−21.0) × 10^3 cm^{-1} for **1a** and (17.0−18.0) × 10^3 cm^{-1} for **1b**,

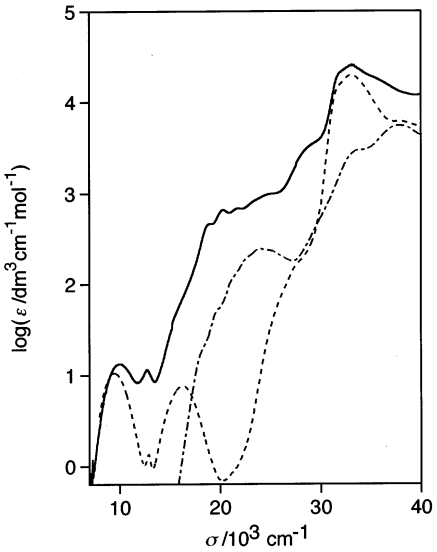

Figure 6. Absorption spectra of $[Ni(acac)_2(IM2py)]$ (**1b**) (−), $[Ni(acac)_2(tmen)]$ (− −), and IM2py (− - −) in CH_2Cl_2 at room temperature.

significant intensity enhancements were observed, especially for the vibrational bands at 1545 and 1480 cm^{-1}, which can be assigned to the N−O stretching vibrations of the O−N=C moiety in the IM2py ligand. The remaining enhanced peaks at 340 and 630 cm^{-1} for **1a** and at 255 cm^{-1} for **1b** may be due to Cr−N,N and Ni−N,N stretching, respectively. Thus, the observed resonance enhancements of the Raman bands lead to the assignment of the shoulders around (19−20) × 10^3 cm^{-1} for **1a** and (17.0−18.0) × 10^3 cm^{-1} for **1b** to the charge-transfer transition.

The absorption intensity enhancement on lowering the temperature for the Cr(III) complex **1a** (Figure 7) substantiates the rigorous assignment to the triplet−triplet metal t_{2g}-to-ligand SOMO π^* (MLCT) transition(Figure 8).

The MLCT intensities of the Ni(II) IM2py complexes are much weaker than those of the Ni(II) NIT2py complexes.[14] This is due to the depopulation of the doublet ground state for the ferromagnetically coupled IM2py Ni(II) complex as supported by the intensity decrease on lowering the temperature as shown in Figure 9. This suggests that the MLCT is not quartet ($t_{2g}-\pi^*$) but doublet ($e_g-\pi^*$), similarly to the Ni(II) NIT2py complexes[14] (Figure 10).

Near-Infrared Absorption Spectra: Spin-Forbidden d−d Transitions. For the radical complexes $[Cr(\beta\text{-diketonato})_2(IM2py)]^+$, the absorption peaks around 14 × 10^3 cm^{-1} were intensified by several hundred times as compared with

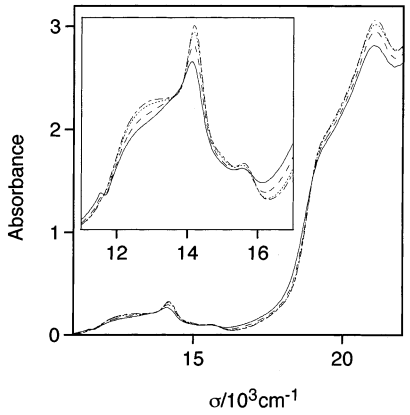

Figure 7. Absorption spectra of $[Cr(acac)_2(IM2\text{-}py)]PF_6$ (**1a**) in an acetate cellulose film at 300 (−), 200 (− − −), 100 (- - -), and 10 K (− - −).

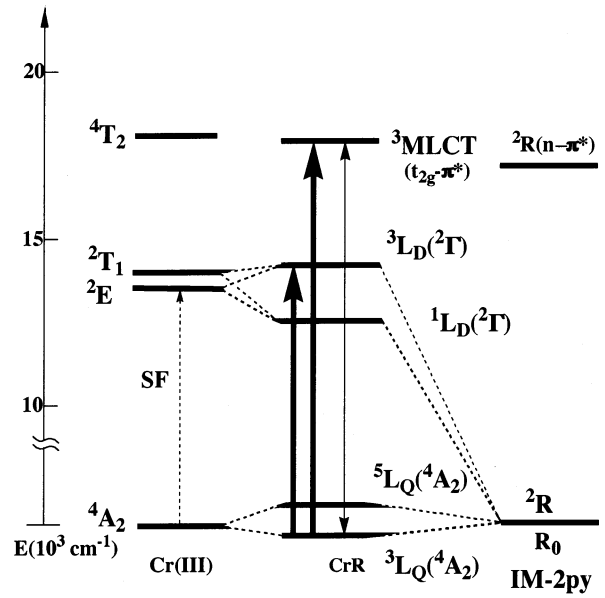

Figure 8. Energy levels of the spin-allowed and spin-forbidden d−d transition: (→) absortion spectra; (→) spin-forbidden absorption; and (↔) configurational interactions between the ground and CT states with the same spin multiplicity.

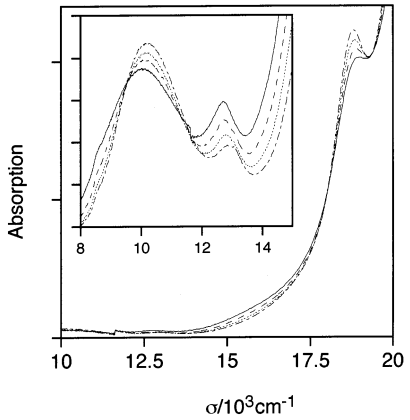

Figure 9. Absorption spectra of $[Ni(acac)_2(IM2py)]$ (**1b**) in an acetate cellulose film at 300 (−), 250 (− - −), 200 (- - -), and 150 K (− - −).

those of the nonradical complex $[Cr(acac)_2(en)]^+$ in the corresponding region as shown in Figure 5. Such enormous intensity enhancements in the spin-forbidden $^4A_2 \rightarrow {}^2E,{}^2T_1$

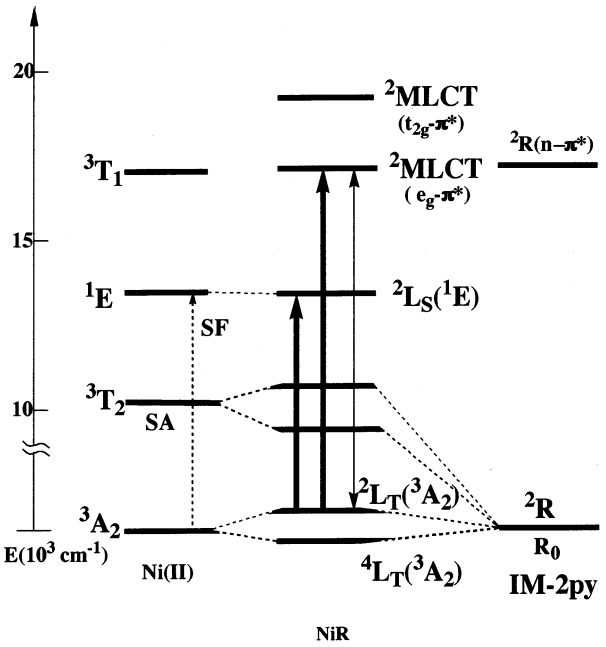

Figure 10. Energy levels of the spin-allowed and spin-forbidden d−d transition: (→) absortion spectra; (→) spin-forbidden absorption; and (↔) configurational interactions between the ground and CT states with the same spin multiplicity.

d−d transitions are ascribed to the exchange coupling between Cr(III) and the IM2py.

The exchange coupling of the ground $^4A_2$ and the excited $^2\Gamma$ (Γ = E and/or T_1) states with the IM2py radical gives the triplet ^3L_Q ($^4A_2$), the quintet ^5L_Q ($^4A_2$) and the triplet ^3L_D ($^2\Gamma$), the singlet $^1L_D(^2\Gamma)$ states as shown in Figure 8. Therefore, the quartet−doublet spin-forbidden d−d transitions of $[Cr(\beta\text{-diketonato})_2(IM2py)]^+$ become formally spin-forbidden or substantially spin-allowed between the exchange coupled triplets as a result of the breakdown of $\Delta S = 0$ restriction. This assignment is supported by the absorption band intensity enhancement on lowering the temperature (Figure 7), in accordance with the antiferromagnetic interaction observed by the variable-temperature magnetic susceptibility measurements.

For $[Ni(\beta\text{-diketonato})_2(IM2py)]$, the absorption intensities originating from the spin-forbidden $^3A_2 \rightarrow {}^1E$ d−d transitions around 13×10^3 cm^{-1} were enhanced by several tens of times as compared with those of the nonradical complex $[Ni(acac)_2(tmen)]$ as shown in Figure 6. The exchange couplings in the ground $^3A_2$ state and the excited ^1E state with the IM2py lead to the $^4L_T(^3A_2)$, the $^2L_T(^3A_2)$, and the $^2L_S(^1E)$ states as shown in Figure 10. This results in the breakdown of the $\Delta S = 0$ restriction by which the triplet−singlet transitions become spin-allowed between the exchange-coupled doublets. This assignment is substantiated by the absorption band intensity diminution on lowering the temperature (Figure 8), resulting from the Boltzmann depopulation of the doublet level in the ground state, in agreement with the ferromagnetic interaction observed by the magnetic susceptibility measurements (vide supra). As compared with the NIT2py Ni(II) complexes, the intensities of the IM2py Ni(II) complexes were much smaller. The large difference

(ϵ_{SF}(IM2py) = 4.86−11.6 dm^3 cm^{-1} mol^{-1}; ϵ_{SF}(NIT) = 111−465 dm^3 cm^{-1} mol^{-1}) between the two series reflects the difference in magnetic interaction.

Changes of the absorption band intensity on lowering the temperature for the Cr(III) and Ni(II) complexes do not reproduce the magnetic coupling constants (J) estimated from the magnetic susceptibility measurements as is similarly found for the corresponding NIT2py complexes.[14,16]

The difference in the magnetic and optical properties among the IM2py Cr(III) and Ni(II) complexes with various kinds of β-diketonates is examined in terms of the exchange mechanism for the intensity enhancement in the formally spin-forbidden d−d transition region of the IM2py complexes as discussed below.

Correlation between the Absorption Intensity and the Magnetic Coupling Constant through the Coligand Effect. According to the exchange mechanism,[30] the spin-forbidden $^3L_Q(^4A_2) \rightarrow {}^3L_D(^2\Gamma)$ and $^2L_T(^3A_2) \rightarrow {}^2L_S(^1E)$ transitions of the IM2py Cr(III) and Ni(II) complexes, respectively, are made allowable by the mixing of the MLCT excited states through the perturbation, i.e., the electron-transfer integral between the Cr(t_{2g})-IM2py(SOMO π^*) and the Ni(e_g)-IM2py(SOMOπ^*) as examined in our previous paper.[14,16] The spin-forbidden transitions attain the transition intensity or the integrated intensity I_{SF} by acquiring a small part ($b = h_{CT}/\Delta E_{CT}$) of that of the spin-allowed MLCT. h_{CT} is the electron-transfer integral: $\langle\Psi_0(^3L_Q(^4A_2))|h^{Cr}|\Phi(^3MLCT)\rangle$ for Cr(III) and $\langle\Psi_0(^2L_T(^3A_2))|h^{Ni}|\Phi(^2MLCT)\rangle$ for Ni(II). ΔE_{CT} is the difference ($E_{CT} - E_{SF}$) between the transition energies where E_{CT} and E_{SF} refer to the transition energies from the triplet ground state to the ^{3}MLCT (E_{CT}) and the $^3L_D(^2\Gamma)$-(E_{SF}) for Cr(III) or those from the doublet ground state to the ^{2}MLCT (E_{CT}) and the $^2L_S(^1E)$ (E_{SF}) for Ni(II). Then, the following equation is given.

$$I_{SF} = b^2 I_{CT} = (h_{CT}/\Delta E_{CT})^2 I_{CT} \quad (1)$$

The configurational interaction with the triplet (Cr) or doublet (Ni) excited MLCT state results in stabilizing the triplet (Cr) or the doublet (Ni) ground-state level by h_{CT}^2/E_{CT} (Figures 8 and 10 and eq 2).

$$J_{AF} = h_{CT}{}^2/E_{CT} \quad (2)$$

$$\approx (I_{SF}/I_{CT})(\Delta E_{CT})^2/E_{CT} \propto (\epsilon_{SF}/\epsilon_{CT})(\Delta E_{CT})^2/E_{CT} \quad (3)$$

Thus, in terms of the ratio of the spin-forbidden transition intensities to the MLCT values[31] from eqs 1 and 2 by considering the antiferromagentic interaction through the charge-transfer integral h_{CT},[30] the exchange coupling constant J_{AF} is expressed as in eq 3.

The integrated intensity I_{SF} in eq 3 may be approximated by the product of the molar absorption coefficient (ϵ) and the half-bandwidth ($\Delta_{1/2}$) as previously proposed.[14,16] The ratios $\epsilon_{SF}/\epsilon_{CT}$[31] are almost constant, and the MLCT transition energy E_{CT}[31] and the energy difference (ΔE_{CT}) between the MLCT and the spin-forbidden transition energy do not change with different kinds of β-diketonates. Accordingly, as shown in Table 4, $(\epsilon_{SF}/\epsilon_{CT})(\Delta E_{CT})^2/E_{CT}$) or J_{AF} is almost constant for variations of β-diketonates, in contrast to the large difference of the J_{obsd} values from ca. −96.4 to −188 cm^{-1} (Cr) or from ca. +0.400 to +95.3 cm^{-1} (Ni) (Table 4). That is, the antiferromagnetic interaction is not affected by the coligands in the two series. Since the J_{obsd} values are the sum of the antiferromagnetic and ferromagnetic contribution, i.e., $J_{obsd} = J_{AF} + J_F$, the variation of the J_{obsd} values seems to reflect that of the J_F values. In other words, in both series the coligand effect may be operative in the ferromagnetic interaction, but not in the antiferromagnetic one. Therefore, the magnetic interactions of the IM2py bis(β-diketonato) Cr(III) and Ni(II) complexes are mainly varied with the change of the ferromagnetic coupling. This behavior is the same as that of the NIT2py Cr(III) complexes,[16] but different from that of the NIT2py Ni(II) complexes.[14]

The hypothetical variation of the J_F values depending on coligands may be accounted for theoretically by considering the lowest quintet LMCT for Cr(III) and the quartet MLCT for Ni(II). The highest or lowest spin multiplet level of the ground state is stabilized due to the configurational interaction, leading to the ferromagnetic or antiferromagnetic or varying the J_F or J_{AF} values, respectively, as in Figures 8 and 10.[32] That is, the ferromagnetic interaction concerns the ^{5}LMCT(HOMOπ-e_g) for Cr(III) and ^{4}MLCT(t_{2g}-π^*) for Ni(II), whereas the antiferromagnetic interaction concerns the ^{3}MLCT(t_{2g}-π^*) for Cr(III) and the ^{2}MLCT(e_g-π^*) for Ni(II).[33] Consequently, the variation in J_{obs} values with the coligand effect can be interpreted by considering the J_F and J_{AF}, namely, both the magnetic orbital orthogonality and overlap. The difference in degree of the electron-transfer integral or overlap integral between the IM2py and NIT2py with the metal d orbitals is compared on the basis of the chelate ring planarity (IM2py being more planar than

(29) Ullman, E. F.; Osiecki, J. H.; Rey, P.; Sessoli, R. *J. Am. Chem. Soc.* **1972**, *94*, 7049.

(30) Ferguson, J.; Guggenheim, H. J.; Tanabe, Y. *J. Phys. Soc. Jpn.* **1966**, *21*, 692.

(31) The positions of the MLCT shoulders were estimated by the second derivatives of the absorption envelope, and the intensities were approximated by the values of the ordinate (molar absorption coefficients) corresponding to those of the estimated abscissa (wavenumber). The difference in the estimated positions and intensities of the MLCT (Table 4) among the β-diketonato complexes may be intrinsic, but does not result from the influence of the shorter wavelength intense intraligand n−π^* transition of the IM2py, since the latter is not so much varied with the β-diketonate coligands.

(32) (a) Kahn, O. *Molecular Magnetism*; VCH Publisher Inc.: New York, 1993; Chapter 8. (b) Tuczek, F.; Solomon, E. I. *Inorg. Chem.* **1993**, *32*, 2850. (c) Tuczek, F.; Solomon, E. I. *Coord. Chem. Rev.* **2001**, *219−221*, 1075−1112.

(33) $\Psi_0(^3L_D(^4A_2))$ and $\Phi_0(^3MLCT)$ for Cr(III) or $\Psi_0(^2L_T(^3A_2))$ and $\Phi_0(^2MLCT)$ for Ni(II) are approximated to represent $|t_{2g}{}^+t_{2g}{}^+t_{2g}{}^+\pi^{*-}|$ and $|t_{2g}{}^+t_{2g}{}^+\pi^{*-}\pi^{*+}|$ or $|(t_{2g})^6e_g{}^+e_g{}^+\pi^{*-}|$ and $|(t_{2g})^6e_g{}^+\pi^{*+}\pi^{*-}|$, respectively. That is, $h_{t\pi^*}{}^{Cr} = \langle\Psi_0(^3L_Q(^4A_2))|h|\Phi_0(^3MLCT)\rangle = \langle|t_{2g}{}^+t_{2g}{}^+\pi^{*-}|h|t_{2g}{}^+t_{2g}{}^+\pi^{*-}\pi^{*+}|\rangle = \langle|t_{2g}{}^+|h|\pi^{*+}|\rangle$ for Cr(III) or $h_{e\pi^*}{}^{Ni} = \langle\Psi_0(^2L_T(^3A_2))|h|\Phi_0(^2MLCT)\rangle = \langle|(t_{2g})^6e_g{}^+e_g{}^+\pi^{*-}|h|(t_{2g})^6e_g{}^+\pi^{*+}\pi^{*-}|\rangle = \langle|e_g{}^+|h|\pi^{*+}|\rangle$ for Ni(II). In a similar manner, the quintet π−e_g LMCT ($|\pi^-t_{2g}{}^+t_{2g}{}^+t_{2g}{}^+e_g{}^+\pi^{*+}|$ from $|\pi^-\pi^+t_{2g}{}^+t_{2g}{}^+t_{2g}{}^+\pi^{*+}|$) and the quartet t_{2g}−π^* MLCT ($|(t_{2g})^4t_{2g}{}^+e_g{}^+e_g{}^+\pi^{*+}\pi^{*-}|$ from $|(t_{2g})^4t_{2g}{}^+t_{2g}{}^-e_g{}^+e_g{}^+\pi^{*+}|$) give the electron transfer integral $h_{e\pi}{}^{Cr} = \langle|e_g{}^+|h|\pi^+|\rangle$ and $h_{t\pi^*}{}^{Ni} = \langle|t_{2g}{}^-|h|\pi^{*-}|\rangle$, respectively. The stabilization of the quintet and quartet level in the ground state or the variation of J_F values could result from the difference in the configurational interaction between the ground and excited states.

NIT2py) as revealed by the X-ray analysis (vide supra). J_F and $|J_{AF}|$ depend on $h_{e\pi}^{Cr} = \langle|e_g^+|h|\pi^+|\rangle$ and $h_{t\pi^*}^{Cr} = \langle|t_{2g}^+|h|\pi^{*+}|\rangle$, respectively, for Cr(III) and $h_{t\pi^*}^{Ni} = \langle|t_{2g}^-|h|\pi^{*-}|\rangle$ and $h_{e\pi^*}^{Ni} = \langle|e_g^+|h|\pi^{*+}|\rangle$,[33] respectively , for Ni(II), assuming that the respective factors $1/E_{CT}$ in eq 2 for J_{AF} and in the analogous equation for J_F are not so much different on going from the NIT2py Cr(III) or the NIT2py Ni(II) complexes to the corresponding IM2py Cr(III) or Ni(II) complexes.

For Cr(III), the overlap between the $e_g(d_\sigma)$ and π orbitals ($h_{e\pi}^{Cr} = \langle|e_g^+|h|\pi^+|\rangle$) or between the $t_{2g}(d_\pi)$ orbitals and the π^* ($h_{t\pi^*}^{Cr} = \langle|t_{2g}^+|h|\pi^{*+}|\rangle$) leads to the relationship $h_{e\pi}^{Cr}$(NIT) > $h_{e\pi}^{Cr}$(IM) or $h_{t\pi^*}^{Cr}$(NIT) < $h_{t\pi^*}^{Cr}$(IM), which gives the following inequalities (eqs 4 and 5).

$$J_F(\text{NIT}) > J_F(\text{IM}) \tag{4}$$

$$-|J_{AF}(\text{NIT})| > -|J_{AF}(\text{IM})| \tag{5}$$

For Ni(II) with the $e_g(d_\sigma)$ magnetic orbital, the situation is completely reverse in terms of the relationship $h_{e\pi^*}^{Ni}$(NIT) < $h_{e\pi^*}^{Ni}$(IM) and $h_{t\pi^*}^{Ni}$(NIT) > $h_{t\pi^*}^{Ni}$(IM);[34]

$$J_F(\text{NIT}) < J_F(\text{IM}) \tag{6}$$

$$-|J_{AF}(\text{NIT})| < -|J_{AF}(\text{IM})| \tag{7}$$

The addition of these inequalities ((4) + (5) and (6) + (7)) leads to the following inequalities.

For Cr(III):

$$-|J_{AF}(\text{NIT})| + J_F(\text{NIT}) > -|J_{AF}(\text{IM})| + J_F(\text{IM})$$

For Ni(II):

$$-|J_{AF}(\text{NIT})| + J_F(\text{NIT}) > |J_{AF}(\text{IM})| + J_F(\text{IM})$$

These are in accordance with the following findings.

For the Cr(III) complexes:

$$J_{obs}(\text{NIT}) > J_{obs}(\text{IM})$$

For the Ni(II) complexes:

$$J_{obs}(\text{NIT}) < J_{obs}(\text{IM})$$

This accounts for the difference in magnetic behavior among the Cr(III) and Ni(II) complexes with IM2py and NIT2py by considering both the antiferromagnetic and ferromagnetic contributions to the J_{obs} through the exchange mechanism. It is seen that the reverse behavior in the inequal relations results from the difference in magnetic orbitals of Cr(III) and Ni(II), $t_{2g}(d_\pi)$ and $e_g(d_\sigma)$, which are orthogonal to each other.

The coligand effect on the J_{obs} or J_F values could arise from the difference in electronic properties of the β-diketonates. The J_{obsd} values of the IM2py Cr(III) and Ni(II) complexes tend to increase on decreasing the acid dissociation exponent pK_a of the β-diketones except for the dbm Cr(III) complex. Thus, the J_F values increase on decreasing the pK_a or increasing the Lewis acidity of the metal sites in the M(β-diketonate)$_2$ moiety, making the interaction between IM2py and metal ions stronger. This may result in an increase of the orbital overlap between the $e_g(d_\sigma)$ and the π^+ for Cr(III) or the $t_{2g}(d_\pi)$ and the SOMO(π^*) for Ni(II), leading to an increase of the ferromagnetic interaction J_F. It is noted that this situation is also found to be the same as that for the NIT2py Cr(III) complexes,[16] but in contrast to the case for the corresponding NIT2py Ni(II) complexes where the J_{AF} values were correlated with the Hammett constant.[14]

Conclusions

The differences in magnetic behavior among the Cr(III) and Ni(II) complexes with IM2py and NIT2py are elucidated by considering the overlaps between the magnetic orbital (t_{2g} or e_g) and the SOMO π^*, LUMO π^*, or HOMO π in the nitroxide radicals.

For the Cr(III) and Ni(II) IM2py complexes, a large variation of J_{obsd} is found to originate from the ferromagnetic interaction (J_F), but not from the antiferromagnetic interaction (J_{AF}) as found for the corresponding Ni(II) complexes[14] on the basis of the exchange mechanism. This coligand effect on J_F arises from the electronic effect of the β-diketonates as revealed from the correlation with the Lewis acidity (pK_a) of the β-diketones themselves. Quantitative elucidation must await further research underway in our laboratory.

Acknowledgment. We gratefully acknowledge support of this research by a Grant-in-Aid for Scientific Research (A) (No.10304056) from the Ministry of Education, Culture, Science and Technology.

Supporting Information Available: Variable-temperature magnetic susceptibilities with each fitting for the two-spin system, UV−vis absorption spectra, resonance Raman spectra for the complexes, and the relation between the J_{obs} values and pK_a, and the magnetic data (Figures 1S−17S and Table 1S), as well as X-ray crystallographic files in CIF format. This material is available free of charge via the Internet at http://pubs.acs.org.

IC011282M